Hindawi
Journal of Mathematics
Volume 2022, Article ID 7929161, 13 pages
https://doi.org/10.1155/2022/7929161

Research Article

An Application of the Finite Element Method for Heat and Mass Transfer of Boundary Layer Flow Using Variable Thermal Conductivity and Mass Diffusivity

Muhammad Shoaib Arif,[1,2] **Kamaleldin Abodayeh**,[1] **and Yasir Nawaz**[2]

[1]*Department of Mathematics and Sciences, College of Humanities and Sciences, Prince Sultan University, Riyadh 11586, Saudi Arabia*
[2]*Department of Mathematics, Air University, PAF Complex E-9, Islamabad 44000, Pakistan*

Correspondence should be addressed to Muhammad Shoaib Arif; maths_zaas@hotmail.com

Received 23 February 2022; Revised 9 August 2022; Accepted 17 August 2022; Published 16 September 2022

Academic Editor: Nauman Raza

Since mass diffusivity and thermal conductivity cannot be considered constants in practical analysis, an existing heat and mass transfer model of unsteady mixed convection flow over a stretching sheet is modified by incorporating the effects of nonlinear mixed convection variable thermal conductivity and mass diffusivity and solved its dimensionless form by applying the finite element method which is the main novelty of this work. Nonlinear governing equations are created because of changing thermal conductivity and mass diffusivity. Nonlinear solutions can be achieved by employing the Galerkin finite element approach. Temperature and concentration-based thermal conductivity and mass diffusivity are considered. The model is expressed as a set of partial differential equations, and furthermore, it is reduced to a system of dimensionless ordinary differential equations. These obtained equations are solved with the finite element method with linear interpolating polynomials and numerical integration. In addition, a Matlab solver bvp4c is also considered for comparison purposes or validation of the computed results. The graphs depict the effect of various parameters on the velocity, temperature, and concentration curves. The results show that thermal and diffusive wave propagation is significantly affected by thermal conductivity and mass diffusivity changes. Results show that flow velocity escalates by rising values of thermal and solutal Grashof numbers.

1. Introduction

A study related to non-Newtonian fluids has gained exquisite attraction due to its massive applications in food and energy, specifically in the petroleum industry. The roots of plastic processing industries peculiarly relied on fluid dynamics in polymer melt and polymer solutions. Industrial slurry multiphase mixers, pharmaceutical formulations, cosmetics and toiletries, paints, biofluids, and food items have become more diverse because of the widespread usage of non-Newtonian fluids. Such studies follow Ostwald-de Waele's power-law model and the boundary layer concept, which was first proposed by Schowalter [1]. Acrivos [2] formulated an extension for the boundary layer non-Newtonian fluid flow in 1960 and leveled the ground for upcoming scholars. Several investigations on chemicals, polymers, and molten plastics have been conducted since then. Many previous investigations of natural convection with transparent fluid media are considered Newtonian fluids by the thermo fluid community. A theoretical analysis of how the shear rate affects convective flow patterns and heat transfer rates in non-Newtonian fluids can be used in papermaking, oil drilling, slurry transport, food processing, and polymer engineering.

Ice formation damage of organs preserves cells and tissues through freezing on the principle of mass and heat transfer. Such studies are essential as non-Newtonian fluids and have robust interference in industries such as petroleum storage, ground-water hydrology, nuclear waste disposal, geothermal energy formation, cooling, and design of solid

matrix heat exchange and packed-bed chemical catalytic reactors. Authors such as Smith et al. [3] were interested in determining mass transfer in rat prostate tumor tissues. In contrast, El-Hakiem and El-Amin [4] first researched the same transfer in a porous material with nonuniform surface heat flow through a vertical plate. An infinite insulated flat plate near a laminar flow of viscoelastic incompressible fluid of low electrical conductivity was solved by Eldabe and Hassan [5]. Non-Newtonian elastic, viscous fluid flow past an infinite flat plate with changing suction was studied by Soundalgekar and Puri [6].

The theory of non-Newtonian fluid presents the greatest challenge to mathematicians and engineers in developing analytical and numerical solutions for highly nonlinear governing equations. The study for hearing transfer of boundary layer flow over a stretching sheet has been given by Elbashbeshy et al. [7]. A numerical Runge–Kutta method has been considered to handle boundary value problems by Elbashbeshy et al. [7]. The flow was studied with heat generation, chemical reaction, and thermal radiation. The radiation effect was also considered in the boundary layer flow over the exponentially stretching sheet by Nadeem et al. [8]. Two types of effects for heat transfer have been studied: the prescribed exponential order surface temperature and the prescribed exponential order heat flux. An analytical method, namely homotopy analysis, has been utilized to solve differential equations in the radiative flow. It was concluded that the temperature profile was escalated by the growth of the radiation parameter. Both effects of prescribed surface temperature and prescribed heat flux were also studied by Nadeem et al. [9] in the stagnation point flow of third-order fluids.

A shrinking sheet was deliberated with two problems: two-dimensional stagnation point flow over a shrinking sheet and axisymmetric stagnation point flow over axisymmetric shrinking. An analytical technique, homotopy analysis, was adopted to solve the ordinary differential equations. The study of stagnation point flow for a viscous fluid has been given by Nadeem et al. [10]. For the validity of the computed solutions obtained by the homotopy analysis method for solving the boundary layer equation, a comparison with the results obtained by another research was made and found good agreement. Nadeem and Akbar [11] also found an analytical solution for the peristaltic motion of the non-Newtonian incompressible Johnson Segalman fluid. The perturbation and homotopy analysis methods were adopted to tackle the differential equations arising in the studied flow. Nadeem and Ali [12] also employed the homotopy analysis method to solve flow phenomena of the steady incompressible fourth-grade fluid down a vertical cylinder. Variable viscosity and heat transport were also taken into account in the study. Buongiorno [13] used Brownian diffusion and thermophoresis slip mechanisms to develop the nonhomogeneous equilibrium model.

A bounded domain with two-dimensional flows was investigated. Global in-time solutions exist and are unique according to Lukaszewicz [14] and their convergence to the stationary solution for viscous flows. Shenoy [15] presented many exciting applications of non-Newtonian power-law fluids. Together with streamlines and turbulence, mathematical models were studied by Astarita and Marrucci [16] and Bohme [17]. The non-Newtonian power-law fluid with heat transfer over a continuously moving flat porous plate has been analyzed by Kishan and Reddy [18]. The numerical solution was found by employing the implicit finite difference method. The solution was found to be dependent on involved dimensionless parameters. The effects of parameters on velocity and temperature profiles were carried out. Kavitha and Kishan have investigated a radiative boundary layer flow with heat transfer characteristics over a vertical stretching sheet under the effect of viscous dissipation [19]. Some obtained results were compared with existing results and found good agreement.

Nanotechnology dealt with materials of a nanometer in size and gravitated attention due to their unique physical and chemical properties. Fluids comprising small-scaled unit particles are called nanofluids, and heat transfer through such fluids could enhance conductivity. It is the most relevant, innovative technology dealing with the suspension of solid nanoparticles ranging from 1 to 100 nm in diameter within common liquids such as water, oil, and ethylene glycol. A rise in thermal conductivity by 40% can be obtained by decreasing the number of solid nanoparticles in suspension by 1–5% by volume. It depends on solid nanoparticles' size, shape, and thermal properties. The composition of these nanoparticles used in nanofluids is metals, oxides, carbides, and nanotubes. Water, ethylene glycol, and oil are all examples of base liquids. To reduce boiler flue gas temperatures and microelectronic noise, nanofluid technology can be used in various heat transfer applications, such as nuclear reactor coolants, pharmaceutical processes, and boiler flue gas cooling. Such fluids raised the convection and conductivity of heat transmission counterbalance with base fluids. The application of these fluids as heat exchanger plants and automotive cooling systems has been reported by Nadeem et al. [20].

The term nanofluid was first proposed by Choi [21], while its properties such as stability, pressure drop, and passage through nanochannels were given by Zhou [22]. Xuan and Li [23] suggested a mechanism to reduce heat transmission among nanofluids by increasing volume fractions and resultant viscosity. Therefore, selecting a particular nanoparticle regarding its fractional volume substantially enhances conductivity. In addition, Buongiorno [13] introduced the term absolute velocity for nanoparticles which he reckoned by the sum of base fluid velocity and relative velocity (slip velocity). All seven mechanisms he studied included inertia, Brownian diffusion, thermophoresis, the Magnus effect, and fluid drainage and gravitational settling.

(Pak and Cho [24], Wen and Ding [25], Ding et al. [26]) Utilizing nanofluids to promote forced convective heat transfer has been suggested. Alternatively, the mechanism behind this forced convective heat transfer and its characteristics were not elaborated. Due to its efficient convection, the topic of nanofluid has attracted a lot of attention in recent years [27]. Recent research [28, 29] on nanofluids has shown that the heat conductivity rises with decreasing grain size. This was proved through the use of measurements. In Chengara et al. [30], they explore how the disjoining

pressure exerted by nanoparticles in a liquid film affects its spreading. Critical heat fluxes in boiling conditions increase (You et al. [31]). Convection of heat over a permissible elastic wall in a porous medium was investigated by Sheikholeslami et al. [32].

Extrusion, wire drawing, glass fiber manufacture, continuous casting, crystal growth, and paper formation are among the engineering applications that have drawn researchers' attention to boundary layer flow and heat transmission over a constantly stretched surface. Crane [33] was the one who pioneered the study of boundary layer flow over an elastic sheet with variable velocity. In contrast, the convection aspect of the former problem was resolved by Carragher and Crane [34]. Temperature differences on surfaces and fluids were directly related to distances from fixed points [34].

The introduction of nanofluids to fluid dynamics, which owned the property of effective thermal conductivity, created a chance to study non-Newtonian fluids under the roof of nanofluids for effective conductivity. Non-Newtonian nanofluid transport in various geometries and boundary conditions in porous and non-porous media has only been studied by a few researchers. The importance of non-Newtonian nanofluids in physical and biological systems, specifically in polymer melts and paints, is evident from [35–37], which significantly lifted this area for research purposes. These phenomena are found in physics, geophysics, astronomy, and chemical engineering applications, including crystal magnetic damping control, hydromagnetic chromatography, and conducting flow in trickle-bed reactors [38].

Various authors studied the effect of dimensionless parameters on the flows over plates. Asjad et al. [39] worked on MHD nanofluid flow over an exponentially stretching sheet by studying microorganisms and the effects of thermal radiations, chemical reactions, and heat source dissipation. The differential equations obtained from the flow problems were solved using the shooting method based on the Runge–Kutta scheme. The study of microorganisms for mixed convection of Casson nanofluid flow in the stagnation region of the rotating sphere was given in [40]. Gyrotactic microorganisms have been considered to enhance heat transportation, and nano-sized particles were brought into the study to improve stability. The dimensionless partial differential equations were solved by the Galerkin finite element method. The study of microorganisms was also presented for MHD Williamson nanofluid flow [41] over the sheet with irregular thickness. The impacts of temperature-dependent thermal conductivity and nonuniform viscosity were also studied with the aforementioned flow phenomenon. The reduced set of ordinary differential equations was solved by the shooting method. The study of Reiner–Rivlin fluid over a disk has been presented in [42] with Brownian motion and thermophoresis effects.

For simulating MHD Casson flow over a linearly shrinking/stretching sheet, the experimental relations for approximating the thermophysical properties of hybrid nanofluids have been explored in [43]. A fourth-order accurate solution was found using Matlab. The dual solution and stability analysis were also given. The results show that the Casson fluid parameter range enhances with second nanoparticle mass, suction parameter, and radiation parameter. The study of MHD stagnation-point flow over a wavy circular cylinder has been given in [44], considering aluminum-copper/water hybrid nanofluid as the working fluid with temperature jump and velocity slip boundary conditions. The obtained results revealed that a developed mass-based model can be employed further to study heat transfer of hybrid nanofluid flow in similar problems. A semianalytical study for two-dimensional boundary layer flow over a shrinking/stretching wedge has been given in [45]. The Tiwari–Das model with a combination of mass-based hybrid nanofluid procedures was applied to find governing equations of the considered flow problem. It was observed that the boundary layer thickness for the first solution was thinner than the second one. The steady laminar, incompressible, and two-dimensional hybrid nanofluid flow has been studied numerically in [46]. The effects of the convectively-warmed moving wedge with radiative transition have also been considered. The three primary geometries namely the flat plate, the wedge, and the vertical plate were considered. The mass-based method has been combined with the entropy generation analysis for the first time in [46].

The finite element method can adequately predict boundary layer flow's heat and mass transmission profiles. It is the most effective methodology that provides a great understanding of the time history of constitutive variables and is an energetic tool in computational fluid dynamics. In this work, a mathematical model of boundary layer flow is modified using nonlinear mixed convection and studied using the modified finite element method. A summary of each section is given in the next paragraph.

The problem is defined in section 2 with governing equations and boundary conditions, and also in this section, the partial differential equations are transformed into ordinary differential equations using transformations. The procedure for solving equations by the modified finite element method is given in section 3. The validation of the computed results is provided in section 4. The discussion related to graphs is given in section 5.

2. Problem Formulation

Consider incompressible, Newtonian, two-dimensional, and mixed convective unsteady flow over the stretching sheet. Let the sheet be placed horizontally. The x-axis is taken along the sheet, while the y-axis is taken perpendicular to the sheet. The flow is generated by the sudden movement of the plate towards the positive x-axis. Let T be the temperature of the fluid, C be the concentration, $T_w \& C_w$ are respectively temperature and concentration at the wall, and $T_\infty \& C_\infty$ are respectively temperature and concentration at the free stream. The geometry of this problem is given in Figure 1, which shows the direction of flow, coordinate axis and momentum, and thermal and concentration boundary layers. Considering thermal conductivity and mass diffusivity as temperature and concentration-dependent quantities, and following [47–49] the governing equations for this phenomenon can be stated as

$$\frac{\partial u}{\partial x}+\frac{\partial v}{\partial y}=0, \tag{1}$$

$$\frac{\partial u}{\partial t}+u\frac{\partial u}{\partial x}+v\frac{\partial u}{\partial y}=\nu\frac{\partial^2 u}{\partial y^2}+g\left(\Lambda_1\left(T-T_\infty\right)+\Lambda_2\left(T-T_\infty\right)^2+\Lambda_3\left(C-C_\infty\right)+\Lambda_4\left(C-C_\infty\right)^2\right), \tag{2}$$

$$\frac{\partial T}{\partial t}+u\frac{\partial T}{\partial x}++v\frac{\partial T}{\partial y}=\frac{1}{\rho C_p}\frac{\partial}{\partial y}\left(k(T)\frac{\partial T}{\partial y}\right)-\frac{1}{\rho C_p}\frac{\partial q_r}{\partial y}, \tag{3}$$

$$\frac{\partial C}{\partial t}+u\frac{\partial C}{\partial x}+v\frac{\partial C}{\partial y}=\frac{\partial}{\partial y}\left(D(C)\frac{\partial C}{\partial y}\right)-k_1\left(C-C_\infty\right). \tag{4}$$

Subject to the following boundary conditions:

$$\left.\begin{aligned}&u(t,y)=U_w, v(t,y)=v_w, T(t,y)=T_w, C(T,y)=C_w \text{ when } y=0, t>0\\&u(t,y)\longrightarrow 0, T(t,y)\longrightarrow T_\infty, C(T,y)\longrightarrow C_\infty \text{ when } y\longrightarrow\infty, t>0\end{aligned}\right\}, \tag{5}$$

where $k(T)=k_\infty(1+\varepsilon_1(T-T_\infty/T_w-T_\infty)), D(C)=D_\infty(1+\varepsilon_2(C-C_\infty/C_w-C_\infty))$ temperatures, concentration-dependent thermal conductivity, and mass diffusivity have been considered in [50] and equations (1)–(4), and terms having derivatives with respect to x will be ignored, as it is assumed in [47]. $U_w=ax$ denotes the velocity of the stretching sheet, $k(T)$ and $D(C)$ are, respectively, temperatures and concentration-dependent thermal conductivity and mass diffusivity, ν is the kinematic viscosity, g is the gravity, Λ_1 and Λ_2 are the coefficients of linear and nonlinear thermal expansion, respectively, Λ_3 and Λ_4 are coefficients of linear and nonlinear solutal expansions, respectively, ρ is the density of the fluid, C_p denotes the specific heat capacity, k_1 represents the reaction rate, and q_r denotes the radiative flux. In this study, a Rosseland radiative flux [51] is considered, which is expressed as

$$q_r=-\frac{4\sigma^*}{3k^*}\frac{\partial T^4}{\partial y}\approx-\frac{16\sigma^* T_\infty^3}{3k^*}\frac{\partial T}{\partial y}. \tag{6}$$

Consider the following transformations [47].

$$\begin{aligned}\eta&=\frac{y}{\delta(t)},\\u&=U_w f(\eta),\\\theta&=\frac{T-T_\infty}{T_w-T_\infty},\\\phi&=\frac{C-C_\infty}{C_w-C_\infty}.\end{aligned} \tag{7}$$

The continuity equation (1) is solved, and its solution is given by [47].

$$v=-\frac{v_o\nu}{\delta}, \tag{8}$$

where $v_o=-(v_w\delta/\nu)$.

Under transformations (7), equations (2)–(5) are reduced to

$$-f'\left(\eta\frac{\delta\delta'}{\nu}+v_o\right)=f''+G_{r_0}\left(\theta+\beta_1\theta^2\right)+G_{r_m}\left(\phi+\beta_2\phi^2\right)=0, \tag{9}$$

$$-\theta'\left(\eta\frac{\delta\delta'}{\nu}+v_\circ\right)=\frac{1}{P_r}\left(\varepsilon_1\theta'^2+(1+\varepsilon_1\theta)\theta''\right)+\frac{4}{3}\frac{R_d}{P_r}\theta'', \tag{10}$$

$$-\phi'\left(\eta\frac{\delta\delta'}{\nu}+v_\circ\right)=\frac{1}{S_c}\left(\varepsilon_2\phi'^2+(1+\varepsilon_2\phi)\phi''\right)-\gamma\phi, \tag{11}$$

subject to the dimensionless boundary conditions

$$\left.\begin{aligned}&f(\eta)=1, \theta(\eta)=1, \phi(\eta)=1 \text{ when } \eta=0\\&f(\eta)\longrightarrow 0, \theta(\eta)\longrightarrow 0, \phi(\eta)\longrightarrow 0 \text{ when } \eta\longrightarrow\infty\end{aligned}\right\}, \tag{12}$$

where $G_{r_0}=(g\Lambda_1(T_w-T_\infty)\delta^2/U_w\nu), \beta_1=\Lambda_2/\Lambda_1(T_w-T_\infty), G_{r_m}=(g\Lambda_3(C_w-C_\infty)\delta^2/U_w\nu), \beta_2=\Lambda_4/\Lambda_3(C_w-C_\infty), P_r=\rho c_p\nu/k_0, R_d=4\sigma^* T_\infty^3/3k_0k^*, S_c=\nu/D_0, \gamma=k_1\delta^2/\nu$ are thermal Grashof number, nonlinear thermal convection variables, solutal Grashof number, nonlinear solutal convection variables, Prandtl number, radiation parameter, Schmidt number, and dimensionless reaction rate parameter.

To make equations (9)–(11) dimensionless, the following assumption is made [48]:

$$A=\frac{\delta\delta'}{\nu}\text{ is a constant.} \tag{13}$$

Under assumption (13), equations (9)–(11) can be expressed as

$$-f'(\eta A + v_0) = f'' + G_{r_0}\left(\theta + \beta_1\theta^2\right) + G_{r_m}\left(\phi + \beta_2\phi^2\right), \quad (14)$$

$$-\theta'(\eta A + v_0) = \frac{1}{P_r}\left(\varepsilon_1\theta'^2 + (1+\varepsilon_1\theta)\theta''\right) + \frac{4}{3}\frac{R_d}{P_r}\theta'', \quad (15)$$

$$-\phi'(\eta A + v_0) = \frac{1}{S_c}\left(\varepsilon_2\phi'^2 + (1+\varepsilon_2\phi)\phi''\right) - \gamma\phi. \quad (16)$$

The skin friction coefficient is defined as

$$C_f = \frac{\tau}{(1/2)\rho U_w^2}, \quad (17)$$

where $\tau = -\mu(\partial u/\partial y)_{y=0} = -(\mu U_w/\delta)f'(0)$

Therefore,

$$\frac{1}{2}R_e C_f = -f'(0), \quad (18)$$

where $R_e = U_w\delta/\nu$ represents the Reynolds number.

3. Finite Element Method

The problem is more complex because the governing equations for the velocity field are nonlinear. Mathematical equations describe generalized diffusion thermoelasticity concerning changing mass diffusivity and thermal conductivity, including dynamic and nonlinear variables. To solve equations (14)–(16) using boundary conditions (12), a finite element method is employed. The entire domain is partitioned into a finite number of subdomains for this method's implementation. The solution is found at each subdomain. Let N denote the number of subdomains. The first step of the method is to approximate the solution by interpolation polynomials. For the present study, a linear interpolation polynomial is employed. So, let the solution of each equation (14)–(16) be approximated as

$$\begin{aligned} f &= f_0 + f_1\eta, \\ \theta &= \theta_0 + \theta_1\eta, \\ \phi &= \phi_0 + \phi_1\eta, \end{aligned} \quad (19)$$

where $f_0, f_1, \theta_0, \theta_1, \phi_0$, and ϕ_1 are unknown to be found. Let each subdomain be consisting of two nodes located at each end. Let the ith subdomain be denoted by $[\eta_i, \eta_{i+1}]$. When the three interpolated polynomials for each dependent variable are evaluated at ith subdomain, then the resulting solution evaluated at ith subdomain can be expressed as

$$f = \xi_1(\eta)f_i + \xi_2(\eta)f_{i+1}, \quad (20)$$

$$\theta = \xi_1(\eta)\theta_i + \xi_2(\eta)\theta_{i+1}, \quad (21)$$

$$\phi = \xi_1(\eta)\phi_i + \xi_2(\eta)\phi_{i+1}, \quad (22)$$

where $\xi_1(\eta) = (\eta_{i+1} - \eta/\eta_{i+1} - \eta_i), \xi_2(\eta) = (\eta - \eta_i/\eta_{i+1} - \eta_i)$ for $\eta_i \le \eta \le \eta_{i+1}$.

The defined functions $\xi_1(\eta)$ and $\xi_2(\eta)$ are called shape functions, while the dependent variables f, θ, and ϕ are called trial functions. By using the Galerkin approach, weighted residuals for equations (14) to (16) can be expressed as

$$\int_0^{\eta_\infty} \xi\left(\frac{d^2f}{d\eta^2} + (A\eta + v_0)\frac{df}{d\eta} + G_{r_0}\left(\theta + \beta_1\overline{\theta}\theta\right) + G_{r_m}\left(\phi + \beta_2\overline{\phi}\phi\right)\right)d\eta = 0, \quad (23)$$

$$\int_0^{\eta_\infty} \xi\left(\frac{1}{P_r}\left(1 + \frac{4}{3}R_d\right)\frac{d^2\theta}{d\eta^2} + \frac{1}{P_r}\left(\varepsilon_1\overline{\theta}\right)\frac{d^2\theta}{d\eta^2} + \frac{1}{P_r}\varepsilon_1\left(\frac{\overline{d\theta}}{d\eta}\right)\left(\frac{d\theta}{d\eta}\right) + (\eta A + v_0)\frac{d\theta}{d\eta}\right)d\eta = 0, \quad (24)$$

$$\int_0^{\eta_\infty} \xi\left(\frac{1}{S_c}\frac{d^2\phi}{d\eta^2} + \frac{1}{S_c}\left(\varepsilon_2\overline{\phi}\right)\frac{d^2\phi}{d\eta^2} + \frac{1}{S_c}\varepsilon_2\left(\frac{\overline{d\phi}}{d\eta}\right)\left(\frac{d\phi}{d\eta}\right) + (\eta A + v_0)\frac{d\phi}{d\eta} - \gamma\phi\right)d\eta = 0, \quad (25)$$

where $[0, \eta_\infty]$ is the domain of equations (14)–(16). Equations (23)–(25) are strong formulations and weak formulations. The second-order derivative terms are in equations (23)–(25) will be integrated once. This leads to the following weak formulations:

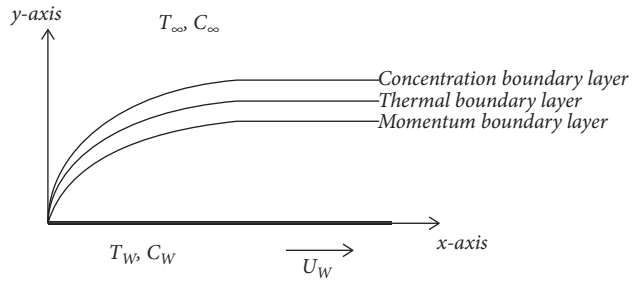

Figure 1: The geometry of the problem.

$$\int_0^{\eta_\infty}\left[-\frac{d\xi}{d\eta}\frac{df}{d\eta}+\xi\left\{(A\eta+\nu_\circ)\frac{df}{d\eta}+G_{r_0}\left(\theta+\beta_1\overline{\theta}\theta\right)+G_{r_m}\left(\phi+\beta_2\overline{\phi}\phi\right)\right\}\right]d\eta=-\left(\frac{\xi df}{d\eta}\right)_0^{\eta_\infty}, \tag{26}$$

$$\int_0^{\eta_\infty}\left[-\frac{1}{P_r}\left(1+\frac{4}{3}R_d\right)\frac{d\xi}{d\eta}\frac{d\theta}{d\eta}-\frac{\epsilon_1\overline{\theta}}{P_r}\frac{d\xi}{d\eta}\frac{d\theta}{d\eta}+\xi\left(\frac{1}{P_r}\epsilon_1\left(\frac{\overline{d\theta}}{d\eta}\right)\left(\frac{d\theta}{d\eta}\right)+(\eta A+\nu_0)\frac{d\theta}{d\eta}\right)\right]=-\left(\xi\frac{d\theta}{d\eta}\right)_0^{\eta_\infty}\frac{1}{P_r}\left(1+\frac{4}{3}R_d\right)-\frac{\epsilon_1\overline{\theta}}{P_r}\left(\xi\frac{d\theta}{d\eta}\right)_0^{\eta_\infty}, \tag{27}$$

$$\int_0^{\eta_\infty}\left[-\frac{1}{S_c}\frac{d\xi}{d\eta}\frac{d\phi}{d\eta}-\frac{1}{S_c}\epsilon_2\overline{\phi}\frac{d\xi}{d\eta}\frac{d\phi}{d\eta}+\xi\left(\frac{1}{S_c}\epsilon_2\left(\frac{\overline{d\phi}}{d\eta}\right)\left(\frac{d\phi}{d\eta}\right)+(\eta A+\nu_0)\frac{d\theta}{d\eta}-\gamma\phi\right)\right]=-\left(\xi\frac{d\phi}{d\eta}\right)_0^{\eta_\infty}\frac{1}{S_c}-\frac{\epsilon_2\overline{\phi}}{S_c}\left(\xi\frac{d\phi}{d\eta}\right)_0^{\eta_\infty}. \tag{28}$$

These weak formulations (26)–(28) are constructed over the whole domain $[0,\eta_\infty]$, and since the finite element method finds the solution on each subdomain, therefore weak formulations on *ith* subdomain are constructed as

$$\int_{\eta_i}^{\eta_{i+1}}\left[-\frac{d\xi}{d\eta}\frac{df}{d\eta}+\xi\left\{(A\eta+\nu_\circ)\frac{df}{d\eta}+G_{r_0}\left(\theta+\beta_1\overline{\theta}\theta\right)+G_{r_m}\left(\phi+\beta_2\overline{\phi}\phi\right)\right\}\right]d\eta=-\left(\frac{\xi df}{d\eta}\right)_{\eta_i}^{\eta_{i+1}}, \tag{29}$$

$$\int_{\eta_i}^{\eta_{i+1}}\left[-\frac{1}{P_r}\left(1+\frac{4}{3}R_d\right)\frac{d\xi}{d\eta}\frac{d\theta}{d\eta}-\frac{\epsilon_1\overline{\theta}}{P_r}\frac{d\xi}{d\eta}\frac{d\theta}{d\eta}+\xi\left(\frac{1}{P_r}\epsilon_1\left(\frac{\overline{d\theta}}{d\eta}\right)\left(\frac{d\theta}{d\eta}\right)+(\eta A+\nu_0)\frac{d\theta}{d\eta}\right)\right]=-\left(\frac{\xi d\theta}{d\eta}\right)_{\eta_i}^{\eta_{i+1}}\frac{1}{P_r}\left(1+\frac{4}{3}R_d\right)-\frac{\left(\epsilon_1\overline{\theta}\right)}{P_r}\left(\frac{\xi d\theta}{d\eta}\right)_{\eta_i}^{\eta_{i+1}}, \tag{30}$$

$$\int_{\eta_i}^{\eta_{i+1}}\left[-\frac{1}{S_c}\frac{d\xi}{d\eta}\frac{d\phi}{d\eta}-\frac{1}{S_c}\epsilon_2\overline{\phi}\frac{d\xi}{d\eta}\frac{d\phi}{d\eta}+\xi\left(\frac{1}{S_c}\epsilon_2\left(\frac{\overline{d\theta}}{d\eta}\right)\left(\frac{d\phi}{d\eta}\right)+(\eta A+\nu_0)\frac{d\phi}{d\eta}-\gamma\phi\right)\right]=-\left(\xi\frac{d\phi}{d\eta}\right)_{\eta_i}^{\eta_{i+1}}\frac{1}{S_c}-\frac{\left(\epsilon_2\overline{\phi}\right)}{S_c}\left(\xi\frac{d\phi}{d\eta}\right)_{\eta_i}^{\eta_{i+1}}. \tag{31}$$

The stiffness matrix for this problem can be expressed as where

$$P^i=\begin{bmatrix}\left[P^{11}\right] & \left[P^{12}\right] & \left[P^{13}\right]\\ \left[P^{21}\right] & \left[P^{22}\right] & \left[P^{23}\right]\\ \left[P^{31}\right] & \left[P^{32}\right] & \left[P^{33}\right]\end{bmatrix}, \tag{32}$$

Table 1: Comparison of the finite element method and Matlab solver *bvp4c* in finding numerical values of $-f'(0)$ using $Gr_m = 1, \beta_1 = 0.1, A = 1, \nu_0 = 1, \varepsilon_1 = 0.1, \varepsilon_2 = 0.1, \gamma = 0.1$.

Gr_0	β_2	R_d	P_r	S_c	$-f'(0)$		Time (s)	
					F.E.M	*bvp4c*	*F.E.M*	*bvp4c*
1	0.5	0.1	0.7	0.7	0.1821	0.2076	0.469	0.324
10					−5.4696	−5.3456	0.451	0.333
0.1	5				−0.7610	−0.7058	0.475	0.343
	0.1	5			0.8283	0.8396	0.432	0.315
		0.1	4		0.9230	0.9345	0.436	0.329
			0.1	4	1.2146	1.2200	0.441	0.348

$$
\begin{aligned}
P_{ij}^{11} &= \int_{\eta_i}^{\eta_{i+1}} \left[-\frac{d\xi_i}{d\eta}\frac{df_j}{d\eta} + \xi_i \left\{ (A\eta + \nu_0)\frac{df_j}{d\eta} \right\} \right] d\eta,\\
P_{ij}^{12} &= \int_{\eta_i}^{\eta_{i+1}} \xi_i \left[G_{r_0}\left(\theta_j + \beta_1 \overline{\theta}\theta_j\right) \right] d\eta,\\
P_{ij}^{13} &= \int_{\eta_i}^{\eta_{i+1}} \xi_i \left[G_{r_m}\left(\phi_j + \beta_2 \overline{\phi}\phi_j\right) \right] d\eta,\\
P_{ij}^{22} &= \int_{\eta_i}^{\eta_{i+1}} \left[-\frac{1}{P_r}\left(1 + \frac{4}{3}R_d\right)\frac{d\xi_i}{d\eta}\frac{d\theta_j}{d\eta} - \frac{\epsilon_1 \overline{\theta}}{P_r}\frac{d\xi_i}{d\eta}\frac{d\theta_j}{d\eta} + \xi_i\left(\frac{1}{P_r}\epsilon_1\left(\frac{\overline{d\theta}}{d\eta}\right)\left(\frac{d\theta_j}{d\eta}\right) + (\eta A + \nu_0)\frac{d\theta_j}{d\eta}\right) \right] d\eta,\\
P_{ij}^{33} &= \int_{\eta_i}^{\eta_{i+1}} \left[-\frac{1}{S_c}\frac{d\xi_i}{d\eta}\frac{d\phi_j}{d\eta} - \frac{1}{S_c}\epsilon_2 \overline{\phi}\frac{d\xi_i}{d\eta}\frac{d\phi_j}{d\eta} + \xi_i\left(\frac{1}{S_c}\epsilon_2\left(\frac{\overline{d\theta}}{d\eta}\right)\left(\frac{d\phi_j}{d\eta}\right) + (\eta A + \nu_0)\frac{d\phi_j}{d\eta} - \gamma\phi_j\right) \right] d\eta.
\end{aligned}
\tag{33}
$$

and the remaining P_{ij}^{mn}, $1 \le m, n \le 3$ are zero. The terms in bar $''-''$ notation are kept fixed to linearize the equations.

4. Validation

An iterative procedure is also considered for the convergence of the solution obtained by employing the finite element method. The iterative solver is employed due to the nonlinearity of the differential equations. This iterative technique begins, finds the solution using the finite element method, and stops if the specified stopping criteria are satisfied. The stopping criteria for the solver are

$$\left| F_{i,j}^{c} - F_{i,j}^{p} \right| < \text{tol}, \tag{34}$$

where $F_{i,j}^{c}$ denotes the solution for one of three dependent variables f, θ, ϕ where $j = 1, 2, 3$ and each grid point i. Suppose the solution obtained at current and previous iterations is not close enough. In that case, the iterative procedure will continue, and it will continue until the obtained values at two consecutive iterations and each grid point are small enough. So, if the iterative method stops, a converged solution may expect.

Also, the results computed by the finite element method are compared with those obtained by Matlab solver bvp4c. This Matlab solver is used to find the solution of linear and nonlinear ordinary differential equations. Using a collocation formula and collocation polynomial, the solver generates a fourth-order accurate continuous solution C^1 using the three-stage Lobatto-IIIa formula. The results for $-f'(0)$ are given in Table 1 using different values of involved parameters. The comparison between results can be seen in Table 1. The numerical values for $-f'(0)$ are calculated by employing two different numerical methods. Also, the comparison of consumed time calculated by employing two different approaches is made in Table 1. The Matlab solver *bvp4c* consumed less time than the considered finite element method.

5. Results and Discussions

The finite element method is employed for solving equations (14)–(16) using boundary conditions (12). The Galerkin finite element method is applied in which weighted residuals of a specific type are constructed, and linear interpolation polynomials are used. Interpolated polynomials are evaluated at two nodes of the subdomain, and shape functions are found. The weak formulations have an advantage over strong formulations, for the approach uses linear interpolating polynomials. For the standard finite element method, the numerical derivatives of solutions are not high-order accurate when interpolation is performed using linear polynomials. However, in the modified approach proposed in [41], numerical derivatives are found using finite difference formulas. So, in this study, a standard approach of the finite element

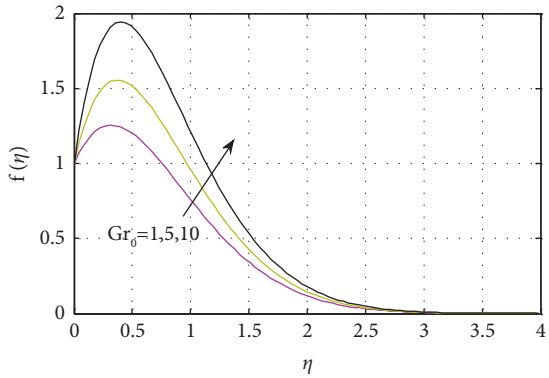

Figure 2: Impact of the thermal Grashof number on the velocity profile using $A = 1, \nu_0 = 0.1, Gr_m = 5, \varepsilon_1 = 0.1, \beta_1 = 0.4, Gr_0 = 5, P_r = 4, R_d = 0.1, S_c = 1.5, \gamma_1 = 0.4$.

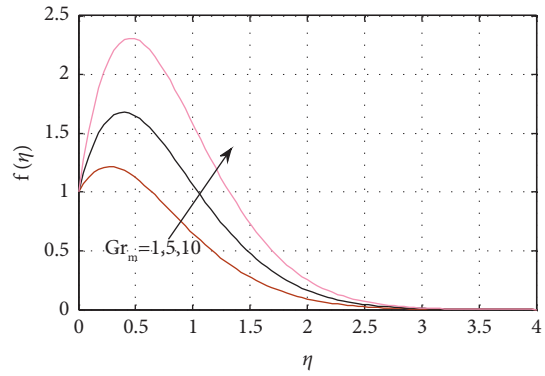

Figure 3: Impact of the solutal Grashof number on the velocity profile using $A = 1, \nu_0 = 0.1, \varepsilon_1 = 0.1, \varepsilon_2 = 0.1, \beta_1 = 0.4, \beta_2 = 0.4, Gr_0 = 5, P_r = 4, R_d = 0.1, S_c = 1.5, \gamma_1 = 0.4$.

method is employed for finding the solutions of equations (14)–(16) using boundary conditions (12), and the numerical values of $-f'(0)$ are found using the modified approach.

Figure 2 shows the velocity profile by varying thermal Grashof number Gr_0. The velocity profile escalates by enhancing the thermal Grashof number. This increase is the increment in the buoyancy force that augments the velocity profile. Figure 3 shows the impact of the solutal Grashof number on the velocity profile. The velocity profile increases by rising solutal (modified) Grashof number values. Mathematically, the rise in the solutal Grashof number increases the flow's acceleration, and consequently, the velocity profile escalates. Figure 4 shows the velocity profile by increasing the parameter ε_1. The velocity profile escalates by the rising values of the parameter ε_1. The increase in the parameter ε_1 escalates the coefficient of dimensionless temperature and yields an increase in thermal conductivity. For mixed convective flows, the temperature is one of the applied forces to initiate or escalate the flow's velocity; therefore, velocity increases. Figure 5 deliberates the velocity profile with the variation of nonlinear thermal convection parameters. The velocity profile increases with the escalation of the

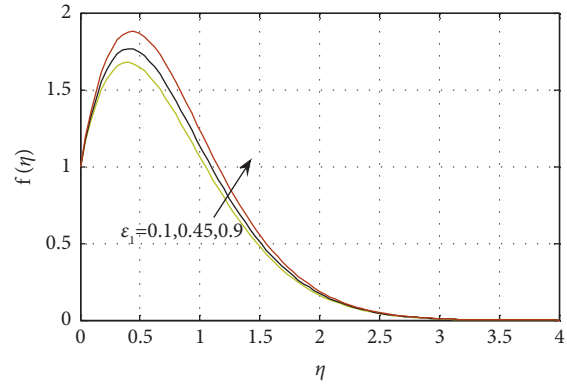

Figure 4: Impact of the parameter in variable thermal conductivity on the velocity profile using $A = 1, \nu_0 = 0.1, Gr_0 = 5, \varepsilon_2 = 0.1, Gr_m = 5, \beta_1 = 0.4, \beta_2 = 0.4, P_r = 4R_d = 0.1, S_c = 1.5, \gamma_1 = 0.4$.

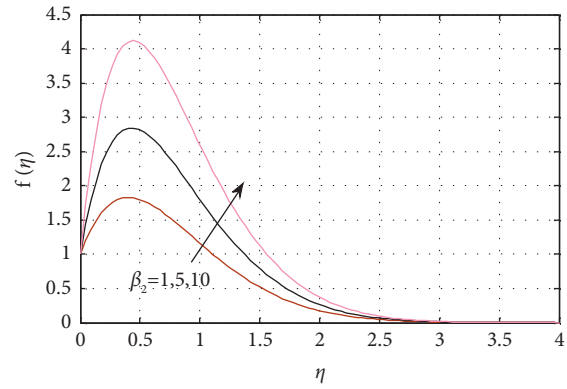

Figure 5: Impact of the nonlinear solutal convection parameter on the velocity profile using $A = 1, \nu_0 = 0.1, Gr_0 = 5, \varepsilon_1 = 0.1, \varepsilon_2 = 0.1, \beta_1 = 0.4, \beta_2 = 0.4, Gr_m = 5, P_r = 4, R_d = 0.1, S_c = 1.5, \gamma_1 = 0.4$.

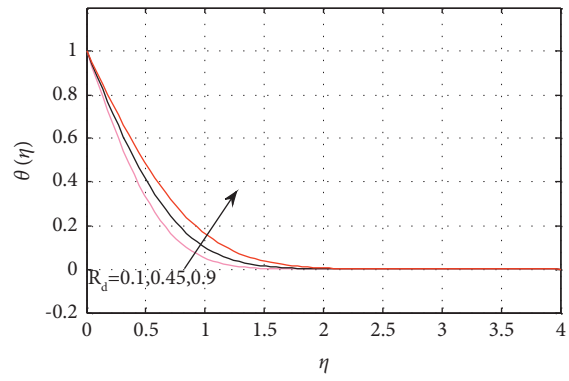

Figure 6: Impact of the radiation parameter on the temperature profile using $A = 1$, $\nu_0 = 0.1$, $Gr_0 = 5$, $\varepsilon_1 = 0.1$, $\varepsilon_2 = 0.1$, $\beta_1 = 0.4$, $\beta_2 = 0.4$, $Gr_m = 5$, $P_r = 4$, $R_d = 0.1$, $S_c = 1.5$, $\gamma_1 = 0.4$.

nonlinear thermal convection parameter. This is due to an increase in the temperature of the flow by enhancing the thermal convection parameter that leads to augments in the velocity profile. The temperature profile with the variation of the radiation parameter is deliberated in Figure 6. The temperature profile grows with the rise in the

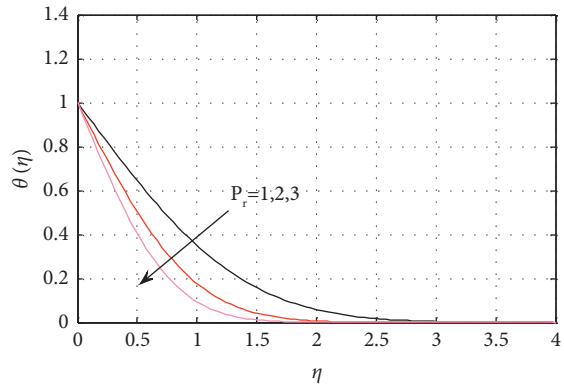

Figure 7: Impact of the Prandtl number on the temperature profile using $A = 1, \nu_0 = 0.1, Gr_0 = 5, \varepsilon_1 = 0.1, \varepsilon_2 = 0.1, \beta_1 = 0.4, \beta_2 = 0.4, Gr_m = 5, R_d = 0.1, S_c = 1.5, \gamma_1 = 0.4$.

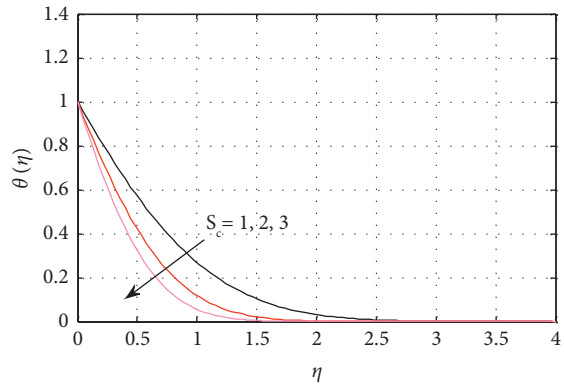

Figure 8: Impact of the Schmidt number on the concentration profile using $A = 1, \nu_0 = 0.1, Gr_0 = 5, \varepsilon_1 = 0.1, \varepsilon_2 = 0.1, \beta_1 = 0.4, \beta_2 = 0.4, Gr_m = 5, R_d = 0.1, P_r = 4, \gamma_1 = 0.4$.

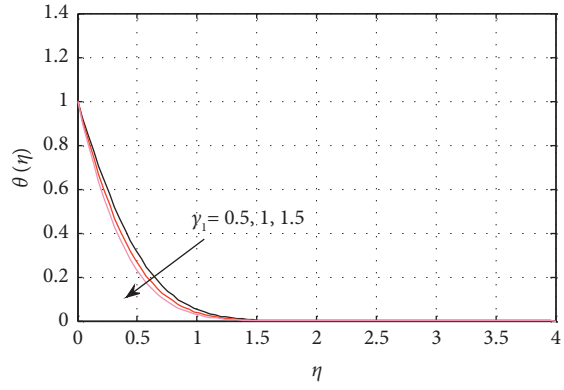

Figure 9: Impact of the reaction rate parameter on the concentration profile using $A = 1, \nu_0 = 0.1, Gr_0 = 5, \varepsilon_1 = 0.1, \varepsilon_2 = 0.1, \beta_1 = 0.4, \beta_2 = 0.4, Gr_m = 5, R_d = 0.1, S_c = 1.5, P_r = 4$.

radiation parameter. This is the consequence of incoming radiations, which escalates in surface heat flux, and therefore, the temperature of the flow rises. Figure 7 deliberates the temperature profile by the change in the Prandtl number. The temperature profile decays by raising the Prandtl number. The growth in the temperature profile is the consequence of thermal conductivity that enhances by the escalation in thermal diffusivity due to increasing values of the Prandtl number. Figure 8 illustrates the effect of the Schmidt number on the concentration distribution. By increasing the Schmidt number, the concentration profile decreases. This increase is the growth of mass diffusivity by escalating the Schmidt number, leading to deescalation in the concentration profile. Figure 9 shows

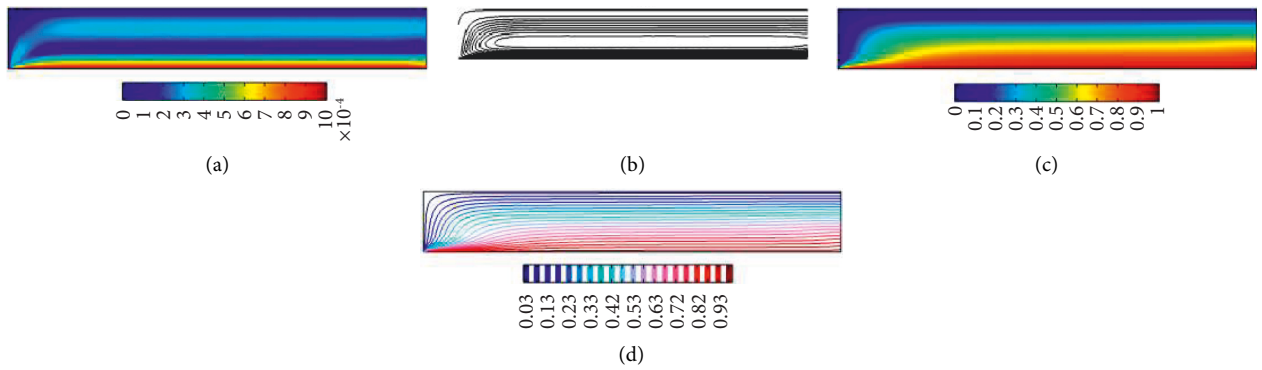

Figure 10: (a) Surface plot for velocity, (b) streamlines, (c) surface plot for temperature, and (d) isothermal contours using $Gr_0 = 100, \beta_1 = 0.7, Gt_m = 0, U_w = 0.001$.

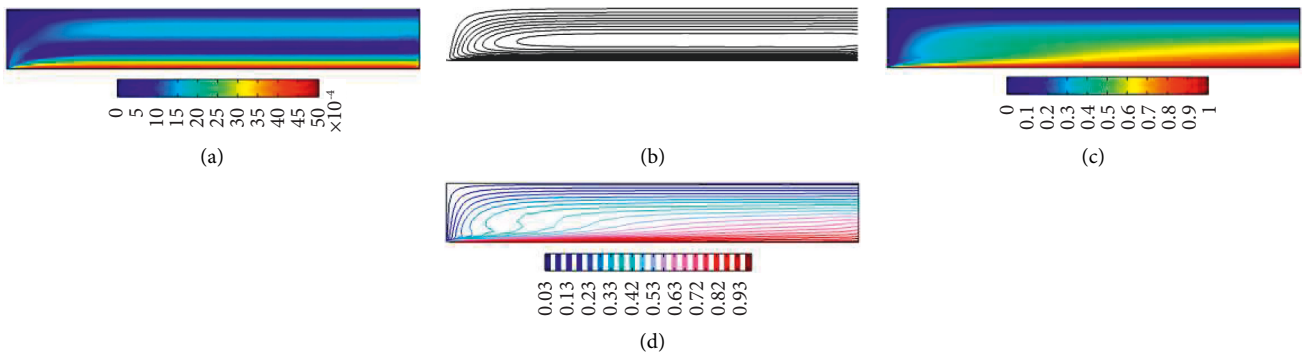

Figure 11: (a) Surface plot for velocity, (b) streamlines, (c) surface plot temperature, and (d) isothermal contours using $Gr_0 = 100, \beta_1 = 0.7, Gr_m = 0, U_w = 0.005$.

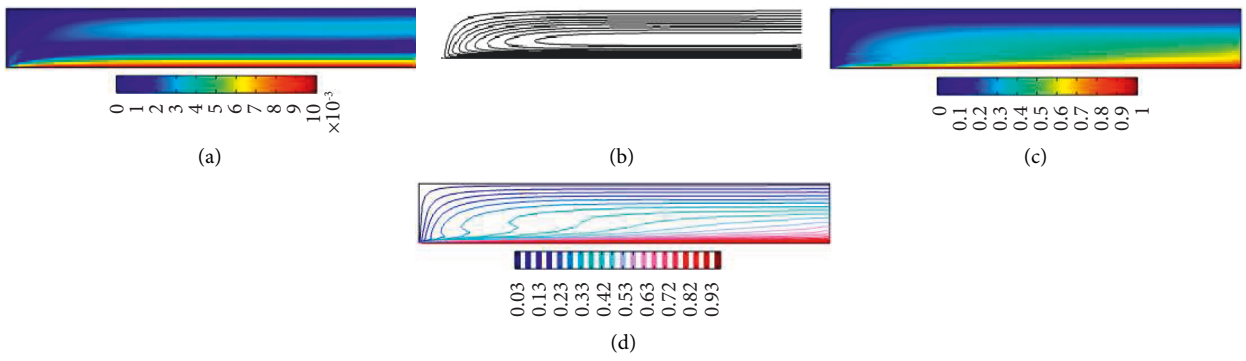

Figure 12: (a) Surface plot for velocity, (b) streamlines, (c) surface plot temperature, and (d) isothermal contours using $Gr_0 = 100, \beta_1 = 0.7, Gr_m = 0, U_w = 0.01$.

the effect of a chemical reaction parameter on the concentration profile. The concentration profile deescalates by the growth of the reaction rate parameter. This decay in the concentration profile is the consequence of either increasing the level of impurity or escalation of creating substances in the flow.

Figures 10–12 are drawn using the partial differential equations as governing heat transfer equations in mixed convection flow under the effect of radiations. The software uses the specified geometry and finds the solution using the finite element method. The considered flow problem's geometry is a rectangle with one inlet and one outlet. The plate is considered to be the lower boundary of the rectangular region. The bottom wall of the rectangular region has a fixed temperature. The water is used as the base fluid. Instead of using the fixed velocity of the sheet, different velocities of the sheet are chosen, and corresponding to each velocity of the sheet, one of the

Figures 10–12 is obtained. The variation in temperature surface plots can be seen in these Figures 10–12 with growing values of the velocity of the wall.

6. Conclusion

Many experimental and theoretical studies show that thermal conductivity and mass diffusivity are not constants. Inspired by these findings, an existing mathematical model for heat and mass transfer flow has been modified. A numerical approach has been employed for solving ordinary differential equations. The nonlinear equations have been linearized, and an iterative procedure has been considered to handle nonlinearities in the equations. Numerical integration of three point formula has been carried out using the Legendre polynomial. The variations of thermal and solutal Grashof numbers, a nonlinear solutal convection parameter, a small parameter in variable thermal conductivity, the Prandtl number, a radiation parameter, the Schmidt number, and a reaction rate parameter on velocity, temperature, and concentration profiles have been presented in the form of graphs. The concluded points can be expressed as

(i) Velocity profile escalated by enhancing thermal and solutal Grashof numbers

(ii) Velocity profile has grown by rising values of nonlinear solutal convection parameters

(iii) Temperature profile escalated by growing values of radiation parameters

(iv) Concentration profile deescalated by augmenting the reaction rate parameter

Furthermore, the modified finite element method considered in this work can be employed to solve nonlinear problems of a similar type that arise in computational fluid dynamics with some extra effects. Following the completion of this work, it will be possible to propose other applications for the currently employed methodology, if desired [52–56]. In addition, the developed method is easy to use and can solve a broader range of differential equations in both practice and theory.

Data Availability

The manuscript included all required data and implementing information.

Conflicts of Interest

The authors declare no potential conflicts of interest concerning this article's research, authorship, and publication.

Acknowledgments

The authors wish to express their gratitude to Prince Sultan University for facilitating the publication of this article through the Theoretical and Applied Sciences Lab. The authors would like to acknowledge the support of Prince Sultan University for paying the Article Processing Charges (APC) of this publication.

References

[1] W. R. Schowalter, "The application of boundary layer theory to power-law pseudoplastic fluid: similar solutions," *AIChE Journal*, vol. 6, pp. 24–28, 2004.

[2] A. Acrivos, "On laminar boundary layer flows with a rapid homogeneous chemical reaction," *Chemical Engineering Science*, vol. 13, pp. 57–62, 1960.

[3] D. J. Smith, R. Devireddy, and J. C. Bischof, *The Archaeological Journal*, vol. 45, no. 3, pp. 639–654, 1999.

[4] M. A. El-Hakiem and M. F. El-Amin, *Heat and Mass Transfer*, vol. 37, no. 2/3, pp. 293–297, 2001.

[5] N. T. M. Eldabe and A. A. Hassan, *Indian Journal of Physics*, vol. 66, p. 359, 1992.

[6] V. M. Soundalgekar and P. J. Puri, "On fluctuating flow of an elastico-viscous fluid past an infinite plate with variable suction," *Journal of Fluid Mechanics*, vol. 35, no. 3, pp. 561–573, 1969.

[7] E. M. A. Elbashbeshy, T. G. Emam, and M. S. Abdel-wahed, "Three—dimensional flow over a stretching surface with thermal radiation and heat generation in the presence of chemical reaction and suction/injection," *International Journal of Energy Technology*, vol. 16, pp. 1–8, 2011.

[8] S. Nadeem, T. Hayat, M. Y. Malik, and S. A. Rajput, "Thermal radiations effects on the flow by an exponentially stretching surface: a series solution," *Zeitschrift für Naturforschung*, vol. 65, pp. 1–9, 2010.

[9] S. Nadeem, A. Hussain, and K. Vajravelu, "Effects of heat transfer on the stagnation flow of a third-order fluid over a shrinking sheet," *Zeitschrift für Naturforschung A*, vol. 65, no. 11, pp. 969–994, 2010.

[10] S. Nadeem, A. Hussain, and M. Khan, "Ham solutions for boundary layer flow in the region of the stagnation point towards a stretching sheet," *Communications in Nonlinear Science and Numerical Simulation*, vol. 15, no. 3, pp. 475–481, 2010.

[11] S. Nadeem and N. S. Akbar, "Influence of heat transfer on a peristaltic flow of johnson segalman fluid in a non-uniform tube," *International Communications in Heat and Mass Transfer*, vol. 36, no. 10, pp. 1050–1059, 2009.

[12] S. Nadeem and M. Ali, "Analytical solutions for pipe flow of a fourth grade fluid with Reynold and Vogel's models of viscosities," *Communications in Nonlinear Science and Numerical Simulation*, vol. 14, no. 5, pp. 2073–2090, 2009.

[13] J. Buongiorno, "Convective transport in nanofluids," *Journal of Heat Transfer*, vol. 128, no. 3, pp. 240–250, 2006.

[14] G. Lukaszewicz, "Asymptotic behavior of micropolar fluid flows," *International Journal of Engineering Science*, vol. 41, no. 3-5, pp. 259–269, 2003.

[15] A. V. Shenoy, "non-Newtonian fluid heat transfer in porous media," *Advances in Heat Transfer*, vol. 24, pp. 101–190, 1994.

[16] G. Astarita and G. Marrucci, *Principles of Non Newtonian Fluid Mechanics*, McGraw-Hill, New York, NY, USA, 1974.

[17] H. Bohme, "Non-newtonian Fluid Mechanics," *northholland Series in Applied Mathematics and Mechanics*, Böhme, Gert. Non-Newtonian Fluid Mechanics, Elsevier, 1987.

[18] N. Kishan and B. S. Reddy, "Mhd effects on non-Newtonian power-law fluid past a continuously moving porous flat plate with heat flux and viscous dissippation," *International Journal of Applied Mechanics and Engineering*, vol. 18, pp. 425–445, 2013.

[19] P. Kavitha and N. Kishan, "Mhd flow of a non-Newtonian power-law fluid over a stretching sheet with thermal

radiation, viscous dissipation and slip boundary conditions," *Acta Technica*, vol. 59, pp. 355–376, 2014.

[20] S. Nadeem, A. Riaz, R. Ellahi, and N. S. Akbar, "Effects of heat and mass transfer on peristaltic flow of a nanofluid between eccentric cylinders," *Applied Nanoscience*, vol. 4, pp. 393–404, 2013.

[21] S. U. S. Choi, "Enhancing thermal conductivity of fluids with nanoparticle," *ASME Fluids Eng. Div,* vol. 231, pp. 99–105, 1995.

[22] D. W. Zhou, "Heat transfer enhancement of copper nanofluid with acoustic cavitation," *International Journal of Heat and Mass Transfer*, vol. 47, no. 14-16, pp. 3109–3117, 2004.

[23] Y. Xuan and Q. Li, "Investigation on convective heat transfer and flow features of nanofluids," *Journal of Heat Transfer*, vol. 125, no. 1, pp. 151–155, 2003.

[24] B. C. Pak and Y. I. Cho, "Hydrodynamic and heat transfer study of dispersed fluids with submicron metallic oxide particles," *Experimental Heat Transfer*, vol. 11, no. 2, pp. 151–170, 1998.

[25] D. S. Wen and Y. L. Ding, "Effective thermal conductivity of aqueous suspensions of carbon nanotubes (carbon nanotube nanofluids)," *Journal of Thermophysics and Heat Transfer*, vol. 18, no. 4, pp. 481–485, 2004.

[26] Y. L. Ding, H. Alias, D. S. Wen, and R. A. Williams, "Heat transfer of aqueous suspensions of carbon nanotubes (cnt nanofluids)," *International Journal of Heat and Mass Transfer*, vol. 49, no. 1-2, pp. 240–250, 2006.

[27] H. Masuda, A. Ebata, K. Teramae, and N. Hishinuma, "Alteration of thermal conductivity and viscosity of liquid by dispersed ultra-fine particles, Dispersion of -Al2O3SiO2 and TiO2 ultra-fine particles," *Netsu Bussei*, vol. 7, pp. 227–233, 1993.

[28] P. Keblinski, S. R. E. Phillpot, S. U. S. Choi, and J. A. Eastman, "Mechanisms of heat flow in suspensions of nano-sized particles (nanofluids)," *International Journal of Heat and Mass Transfer*, vol. 45, no. 4, pp. 855–863, 2002.

[29] D. T. Wasan and A. D. Nikolov, "Spreading of nanofluids on solids," *Nature*, vol. 423, no. 6936, pp. 156–159, 2003.

[30] A. Chengara, A. D. Nikolov, D. T. Wasan, A. Trokhymchuk, and D. Henderson, "Spreading of nanofluids driven by the structural disjoining pressure gradient," *Journal of Colloid and Interface Science*, vol. 280, no. 1, pp. 192–201, 2004.

[31] S. M. You, J. H. Kim, and K. H. Kim, "Effect of nanoparticles on critical heat flux of water in pool boiling heat transfer," *Applied Physics Letters*, vol. 83, no. 16, pp. 3374–3376, 2003.

[32] M. Sheikholeslami, R. Ellahi, H. R. Ashorynejad, G. Domairry, and T. Hayat, "Effects of heat transfer in flow of nanofluids over a permeable stretching wall in a porous medium," *Journal of Computational and Theoretical Nanoscience*, vol. 11, no. 2, pp. 486–496, 2014.

[33] L. J. Crane, "Flow past a stretching plate," *Zeitschrift für angewandte Mathematik und Physik ZAMP*, vol. 21, no. 4, pp. 645–647, 1970.

[34] P. Carragher and L. J. Crane, *Zeitschrift für Angewandte Mathematik und Mechanik*, vol. 62, no. 10, pp. 564-565, 1982.

[35] R. Ellahi, M. Raza, and K. Vafai, "Series solutions of non-Newtonian nanofluids with Reynolds model and vogels model by means of the homotopy analysis method," *Mathematical and Computer Modelling*, vol. 55, no. 7-8, pp. 1876–1891, 2012.

[36] R. Ellahi, S. Aziz, and A. Zeeshan, "Non Newtonian nanofluids flow through a porous medium between two coaxial cylinders with heat transfer and variable viscosity," *Journal of Porous Media*, vol. 16, no. 3, pp. 205–216, 2013.

[37] R. Ellahi, "The effects of mhd and temperature dependent viscosity on the flow of non-Newtonian nanofluid in a pipe: analytical solutions," *Applied Mathematical Modelling*, vol. 37, no. 3, pp. 1451–1467, 2013.

[38] K. V. Prasad, K. Vajravelu, and P. S. Datti, "Mixed convection heat transfer over an on-linear stretching surface with variable fluid properties," *International Journal of Non-linear Mechanics*, vol. 45, no. 3, pp. 320–330, 2010.

[39] M. I. Asjad, N. Sarwar, B. Ali, S. Hussain, T. Sitthiwirattham, and J. Reunsumrit, "Impact of bioconvection and chemical reaction on MHD nanofluid flow due to exponential stretching sheet," *Symmetry*, vol. 13, no. 12, p. 2334, 2021.

[40] B. Ali, A. Shafiq, A. Manan, A. Wakif, S. Hussain, and Bioconvection, "Bioconvection: significance of mixed convection and mhd on dynamics of Casson nanofluid in the stagnation point of rotating sphere via finite element simulation," *Mathematics and Computers in Simulation*, vol. 194, pp. 254–268, 2022.

[41] F. Wang, M. I. Asjad, S. U. Rehman et al., "MHD Williamson nanofluid flow over a slender elastic sheet of irregular thickness in the presence of bioconvection," *Nanomaterials*, vol. 11, no. 9, p. 2297, 2021.

[42] B. Ali, L. Ali, S. Abdal, and M. I. Asjad, "Significance of Brownian motion and thermophoresis influence on dynamics of Reiner-Rivlin fluid over a disk with non-Fourier heat flux theory and gyrotactic microorganisms: a Numerical approach," *Physica Scripta*, vol. 96, no. 9, Article ID 094001, 2021.

[43] S. M. Mousavi, M. N. Rostami, M. Yousefi, S. Dinarvand, I. Pop, and M. A. Sheremet, "Dual solutions for Casson hybrid nanofluid flow due to a stretching/shrinking sheet: a new combination of theoretical and experimental models," *Chinese Journal of Physics*, vol. 71, pp. 574–588, 2021.

[44] B. Jabbaripour, M. Nademi Rostami, S. Dinarvand, I. Pop, and I. Pop, "Aqueous aluminium–copper hybrid nanofluid flow past a sinusoidal cylinder considering three-dimensional magnetic field and slip boundary condition," *Proceedings of the Institution of Mechanical Engineers—Part E: Journal of Process Mechanical Engineering*, Article ID 095440892110464, 2021.

[45] M. Izady, S. Dinarvand, I. Pop, and A.. J. Chamkha, "Flow of aqueous Fe2O3–CuO hybrid nanofluid over a permeable stretching/shrinking wedge: a development on Falkner–Skan problem," *Chinese Journal of Physics*, vol. 74, pp. 406–420, 2021.

[46] H. Berrehal, S. Dinarvand, and I. Khan, "Mass-based hybrid nanofluid model for entropy generation analysis of flow upon a convectively-warmed moving wedge," *Chinese Journal of Physics*, vol. 77, pp. 2603–2616, 2022.

[47] K. Maleque, "Unsteady natural convection boundary layer flow with mass transfer and a binary chemical reaction," *British Journal of Applied Science & Technology*, vol. 3, no. 1, pp. 131–149, 2013.

[48] K. A. Maleque, "Effects of combined temperature and depth-dependent viscosity and hall current on an unsteady MHD laminar convective flow due to rotating disk," *Chemical Engineering Communications*, vol. 197, pp. 508–521, 2010.

[49] T. Hayat, Inayatullah, S. Momani, and K. Muhammad, "FDM analysis for nonlinear mixed convective nanofluid flow with entropy generation," *International Communications in Heat and Mass Transfer*, vol. 126, Article ID 105389, 2021.

[50] M. Waqas, W. A. Khan, and Z. Asghar, "An improved double diffusion analysis of non-Newtonian chemically reactive fluid in frames of variables properties," *International*

Communications in Heat and Mass Transfer, vol. 115, Article ID 104524, 2020.

[51] S. Rosseland, *Astrophysik: Auf Atomtheoretischer Grundlage*, Springer, Berlin, Germany, 2013.

[52] Y. Nawaz and M. S. Arif, "An effective modification of finite element method for heat and mass transfer of chemically reactive unsteady flow," *Computational Geosciences*, vol. 24, no. 1, pp. 275–291, 2020.

[53] S. A. Pasha, Y. Nawaz, and M. S. Arif, "The modified homotopy perturbation method with an auxiliary term for the nonlinear oscillator with discontinuity," *Journal of Low Frequency Noise, Vibration and Active Control*, vol. 38, no. 3-4, pp. 1363–1373, 2019.

[54] Y. Nawaz, M. S. Arif, W. Shatanawi, and A. Nazeer, "An explicit fourth-order compact numerical scheme for heat transfer of boundary layer flow," *Energies*, vol. 14, no. 12, p. 3396, 2021.

[55] Y. Nawaz, K. Abodayeh, M. S. Arif, and M. U. Ashraf, "A third-order two-step numerical scheme for heat and mass transfer of chemically reactive radiative MHD power-law fluid," *Advances in Mechanical Engineering*, vol. 13, no. 10, Article ID 168781402110549, 2021.

[56] S.. Dinarvand, "Nodal/saddle stagnation-point boundary layer flow of CuO–Ag/water hybrid nanofluid: a novel hybridity model," *Microsystem Technologies*, vol. 25, no. 7, pp. 2609–2623, 2019.